

25. P. I. Dalko, Ed., *Enantioselective Organocatalysis* (Wiley, Weinheim, Germany, 2006).
26. B. List, Ed., *Asymmetric Organocatalysis: Topics in Current Chemistry Vol. 291* (Springer, New York, 2009).
27. J.-W. Xie et al., *Angew. Chem. Int. Ed.* **46**, 389 (2007).
28. S. H. McCoey, S. J. Connon, *Org. Lett.* **9**, 599 (2007).
29. P. Melchiorre, *Angew. Chem. Int. Ed.* **51**, 9748 (2012).
30. W. Chen, J. F. Hartwig, *J. Am. Chem. Soc.* **135**, 2068 (2013).
31. Materials and methods are available as supplementary materials on Science Online.
32. C. Uyeda, E. N. Jacobsen, *J. Am. Chem. Soc.* **130**, 9228 (2008).
33. J. Tan, C.-H. Cheon, H. Yamamoto, *Angew. Chem. Int. Ed.* **51**, 8264 (2012).

Acknowledgments: We are grateful to the Swiss National Science Foundation for a grant supporting this work (200020_135224). S.K. thanks the Fonds der Chemischen Industrie for support (Chemiefonds-Stipendium). We thank S. Müller for insightful discussions. Structural parameters for a carbamate derived from (*R,R*)-**3a** are available free of charge from the Cambridge

Crystallographic Data Centre under reference number CCDC 933469.

Supplementary Materials

www.sciencemag.org/cgi/content/full/340/6136/1065/DC1
Materials and Methods
Supplementary Text
Tables S1 to S8
References (34–41)

26 February 2013; accepted 15 April 2013
10.1126/science.1237068

Martian Fluvial Conglomerates at Gale Crater

R. M. E. Williams,^{1*} J. P. Grotzinger,² W. E. Dietrich,³ S. Gupta,⁴ D. Y. Sumner,⁵ R. C. Wiens,⁶ N. Mangold,⁷ M. C. Malin,⁸ K. S. Edgett,⁸ S. Maurice,⁹ O. Forni,⁹ O. Gasnault,⁹ A. Ollila,¹⁰ H. E. Newsom,¹⁰ G. Dromart,¹¹ M. C. Palucis,³ R. A. Yingst,¹ R. B. Anderson,¹² K. E. Herkenhoff,¹² S. Le Mouélic,⁷ W. Goetz,¹³ M. B. Madsen,¹⁴ A. Koefoed,¹⁴ J. K. Jensen,¹⁴ J. C. Bridges,¹⁵ S. P. Schwenzer,¹⁶ K. W. Lewis,¹⁷ K. M. Stack,² D. Rubin,^{18†} L. C. Kah,¹⁹ J. F. Bell III,²⁰ J. D. Farmer,²⁰ R. Sullivan,²¹ T. Van Beek,⁸ D. L. Blaney,²² O. Pariser,²² R. G. Deen,²² MSL Science Team‡

Observations by the Mars Science Laboratory Mast Camera (Mastcam) in Gale crater reveal isolated outcrops of cemented pebbles (2 to 40 millimeters in diameter) and sand grains with textures typical of fluvial sedimentary conglomerates. Rounded pebbles in the conglomerates indicate substantial fluvial abrasion. ChemCam emission spectra at one outcrop show a predominantly feldspathic composition, consistent with minimal aqueous alteration of sediments. Sediment was mobilized in ancient water flows that likely exceeded the threshold conditions (depth 0.03 to 0.9 meter, average velocity 0.20 to 0.75 meter per second) required to transport the pebbles. Climate conditions at the time sediment was transported must have differed substantially from the cold, hyper-arid modern environment to permit aqueous flows across several kilometers.

Decades of spacecraft observations of Mars have revealed abundant evidence for past water flows on the basis of a variety of landforms, including deltas, alluvial fans, valley network comparable to terrestrial river valleys, and giant outflow channels carved by catastrophic floods [e.g., (1–3)]. Although martian landforms commonly possess morphology and scaling relationships similar to their counterparts on Earth, the resolution of satellite images is insufficient to reveal sediment particle size, shape, and sorting patterns. Such detailed sedimentary observations are required to confirm that certain martian landforms derived from fluvial processes and provide critical data to perform paleohydrologic modeling. Before the NASA Mars Science Laboratory (MSL) mission, surface observations on Mars occurred at six locations associated with the Viking, Pathfinder, Mars Exploration Rovers, and Phoenix missions. Collectively, observations from surface instruments showed limited evidence for water transport processes at only two sites. At the Pathfinder landing site, observations of aligned and touching boulders were inferred to reflect clast imbrication by high-velocity catastrophic floods (4–6). In Meridiani Planum, centimeter-scale cross-lamination at Eagle and Erebus craters was interpreted to have resulted from shallow surface flows (with velocities of a few tenths of a meter per

second) within an interaeolian dune paleoenvironment (7–9). However, no definitive in situ evidence of a sustained fluvial overland transport system has been encountered by previous landers.

The MSL Curiosity rover arrived at equatorial Gale crater on 6 August 2012 UTC (Fig. 1). The final landing ellipse was chosen in part because of its proximity to Aeolis Mons (known informally as Mt. Sharp), the central, 5-km-high layered mound within Gale crater, but also because it was close to a prominent alluvial fan, the Peace Vallis fan (10, 11). During the first 100 sols of the mission, Curiosity traveled ~400 m from its landing site across the Bradbury Rise toward bedrock exposed at Glenelg (12, 13). Here, we analyze a suite of rocks encountered along this traverse based on data acquired by the Mast Camera (Mastcam) and ChemCam instruments (14–16).

Outcrop Characteristics

The surface of Bradbury Rise is characterized by two distinct elements: a rock pavement of loose clasts (17) (fig. S1) and occasional horizontal to subhorizontal blocks with embedded pebbles. Here we focus on the latter component, which is present within a narrow (~5 m) elevation range, displays generally similar characteristics, and is interpreted as exposures of a distinct geologic unit or facies. This facies consists of thin (<0.1 m thick), co-

herent blocks that appear to have a well-defined base and limited areal outcrop extent (<1 m²). Although the contact with subjacent rocks is not directly observed, the slabs typically form protruding ledges that imply that the substrate is finer in grain size or less indurated, and easily erodes.

Multiple outcrops of these pebble-rich rock slabs were observed along the first 275 m traversed by the rover, with high-resolution Mastcam images acquired at three locations: Goulburn, Link, and Hottah (Fig. 1C). Goulburn was exposed at the landing site by thrust impingement scouring driven by one of the four pairs of descent engines, which removed unconsolidated regolith and revealed the underlying lithified rock (fig. S2). At this location, a horizontal rock layer composed of pebbles and an unresolved finer component was observed. The other two locations, Link and Hottah, were observed within ~100 m of Goulburn, and displayed tilted, fractured pebble-rich rock slabs with sufficient competency to maintain near-vertical faces (Fig. 2A and Fig.

¹Planetary Science Institute, Tucson, AZ 85719, USA. ²Division of Geological and Planetary Sciences, California Institute of Technology, Pasadena, CA 91125, USA. ³Earth and Planetary Science Department, University of California, Berkeley, CA 94720, USA. ⁴Department of Earth Science and Engineering, Imperial College London, London SW7 2AZ, UK. ⁵Geology Department, University of California, Davis, CA 95616, USA. ⁶Los Alamos National Laboratory, Los Alamos, NM 87545, USA. ⁷Laboratoire Planétologie et Géodynamique de Nantes, LPGN/CNRS UMR6112 and Université de Nantes, 44322 Nantes, France. ⁸Malin Space Science Systems, San Diego, CA 92121, USA. ⁹Institut de Recherche en Astrophysique et Planétologie (IRAP), Université de Toulouse/CNRS, 31400 Toulouse, France. ¹⁰Department of Earth and Planetary Sciences, University of New Mexico, Albuquerque, NM 87131, USA. ¹¹Laboratoire de Géologie de Lyon, Université de Lyon, 69364 Lyon, France. ¹²U.S. Geological Survey, Flagstaff, AZ 86001, USA. ¹³Max-Planck-Institut für Sonnensystemforschung, 37191 Katlenburg-Lindau, Germany. ¹⁴Niels Bohr Institute, University of Copenhagen, 2100 Copenhagen, Denmark. ¹⁵Space Research Centre, Department of Physics and Astronomy, University of Leicester, Leicester LE1 7RH, UK. ¹⁶Department of Physical Sciences, The Open University, Milton Keynes MK7 6AA, UK. ¹⁷Department of Geosciences, Princeton University, Princeton, NJ 08544, USA. ¹⁸U.S. Geological Survey, Santa Cruz, CA 95060, USA. ¹⁹Department of Earth and Planetary Sciences, University of Tennessee, Knoxville, TN 37996, USA. ²⁰School of Earth and Space Exploration, Arizona State University, Tempe, AZ 85287, USA. ²¹Center for Radiophysics and Space Research, Cornell University, Ithaca, NY 14853, USA. ²²Jet Propulsion Laboratory, California Institute of Technology, Pasadena, CA 91109, USA.

*Corresponding author. E-mail: williams@psi.edu

†Present address: Department of Earth and Planetary Sciences, University of California, Santa Cruz, CA 95064, USA.

‡MSL Science Team authors and affiliations are listed in the supplementary materials.

3A). At both locations, multiple decimeter-scale slabs outcrop, separated by linear fractures that display vertical offsets of 2 to 10 cm. The exposed block surfaces dip at approximately constant but gentle angles relative to the ground.

In all three outcrops, the resolvable grains range from very coarse sand (diameter 1 mm) to pebbles (diameter 2 to 40 mm; table S1). The grain size distribution (transformed to a phi scale) approximates a normal (Gaussian) distribution and indicates moderately sorted sediment (Fig. 4) (17). The clast size distributions determined from these rocks are truncated because smaller particles are not sufficiently distinct in the Mastcam images; hence, the measured size distribution is somewhat coarser than the actual grain size dis-

tribution within the rocks. In the first 100 sols, the highest-resolution view of this type of rock is from the ChemCam Remote Micro-Imager (RMI, $\sim 50 \mu\text{m}$ per pixel in this case). The RMI images of Link (Fig. 5) do not allow us to determine whether the matrix consists of fine sand or clay-size grains. The matrix between resolvable grains is generally darker-toned and may include interstitial cement as well as fine grains.

On surfaces that appear less dust-covered, both bright (white or translucent) and dark pebbles are present in color Mastcam images (e.g., Figs. 2 and 3 and fig. S2), with up to half visually appearing as black or gray. In grayscale RMI images on Link, about two-thirds of clasts larger than 2 mm are light-toned and the remainder are

dark-toned (Fig. 5). The variability in size, shape, and color of the pebbles in outcrops reflects different clast compositions and likely multiple provenance lithologies.

Within the outcrops, observable clasts are arranged in grain-to-grain contact. Locally grains form tightly packed clusters (Fig. 3C), including in the highest-resolution images of Link where pebbles are in contact with very coarse sand grains (Fig. 5). In Hottah, parallel stratification is evident in a few relatively dust-free cross-sectional surfaces oriented approximately perpendicular to the rover (Fig. 3B). Elongate clasts are commonly aligned parallel to stratification, and in several examples these clasts show imbrication (Fig. 3D). In places, layers of pebbles are separated by finer-grained, recessed layers that form repeating couplets up to 5 cm thick (Fig. 3C).

Most pebbles observed within these outcrops are distinguished by smooth, rounded perimeters and an equant to tabular shape (fig. S3). The roundness of the pebbles is documented in two ways (17) (table S2). Qualitative roundness indices for the majority of pebbles are classified as subrounded or rounded, and the mean quantitative relative roundness is moderate (~ 0.42 in Hottah and ~ 0.44 near Link).

Rounded pebbles observed by MSL differ from the dominantly angular clasts ($> 1 \text{ cm}$) documented at prior martian lander and rover locations (Viking, Pathfinder, and Mars Exploration Rovers). The quantitative roundness of clasts measured here by Curiosity are an order of magnitude higher than reported at Pathfinder (0.083) (18). Clasts at other martian landing sites have been interpreted as a single lithology of volcanic origin with minimal modification by impact cratering and aeolian processes (18–20). The intermediate roundness values for a portion of the particles at the Viking 1 and Pathfinder landing sites, located in circum-Chryse outflow channels, are consistent with high-energy, short-duration abrasion associated with catastrophic flooding (18–20).

Sediment Transport Processes

The sedimentologic characteristics of these outcrops at Gale crater provide insights into sediment transport processes. Bedload collisional processes in flows produce rounding for heterogeneous clasts, and this is a particularly relevant mechanism for rounding the largest size fraction observed (pebbles with long axis of 10 to 40 mm). Sediment transported by traction (bedload) will slide or roll along the bed. Particles transported in a fluid are subjected to mechanical erosion, or abrasion, of the irregular edges of a particle through numerous impacts and grinding, ultimately producing a smooth surface (21, 22).

The particle size, roundness, sorting, and fabric exposed in these rocks lead us to interpret them as water-transported sediment. The clast size and rounded perimeter of pebbles within these rocks are consistent with their classification as fine-pebble fluvial conglomerates (e.g., a coarse-grained sedimentary rock that is commonly

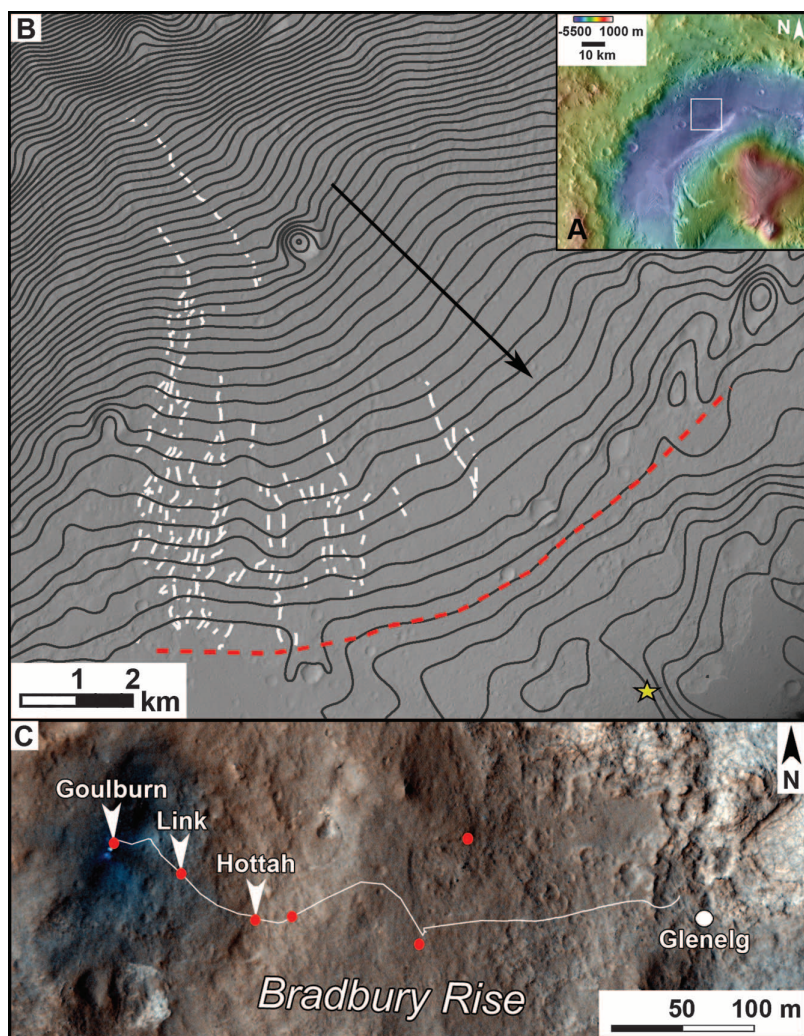


Fig. 1. Location of study site. (A) (inset) The Curiosity rover landed on the Aeolis Palus lowlands in northwestern Gale crater [white box corresponds to (B)]. Color topographic map displays elevation values from the Mars Orbiter Laser Altimeter (MOLA) instrument (39). (B) The Peace Vallis fan is characterized by convex topographic contours (black lines; contour interval is 5 m, arrow marks downslope direction) from smoothed High Resolution Imaging Science Experiment [HiRISE (40)] stereo data. The broad topographic expression of the alluvial fan becomes less distinct downslope of the dashed red line. Sinuous ridges interpreted to record former flow paths (i.e., inverted channels) are mapped in white. Bradbury Rise is marked by yellow star. (C) Curiosity's route in the first 100 sols across Bradbury Rise from the darkened "blast zone" at the landing site toward Glenelg is marked on a HiRISE image (ESP_028335_1755) acquired on 11 August 2012. The locations of pebble conglomerates are marked with red dots.

cemented and made up of rounded to subangular rock fragments larger than 2 mm in diameter in a finer-grained matrix of sand or silt).

Additional evidence for a fluvial interpretation is the stratification at Hottah. Alternating pebble-rich and sand layers (Fig. 3C) indicate fluctuations within sediment transport that result in size sorting of the deposits. In bedload transport, the presence of sand mixed with fine pebbles leads to a sorting instability within flows that produces shallow migrating bedforms (bedload sheets), resulting in fine-scale vertical variations in grain sorting (23), as observed at Hottah.

Alternative sediment transport mechanisms to water flows are inconsistent with the observed rock characteristics. For example, the well-developed rounding of the pebbles together with clast fabric, specifically the grain-to-grain contact and local imbrication, make mass transport as a debris flow unlikely. Likewise, pebble clusters and the relatively wide size range of pebbles within the deposit are inconsistent with transport and deposition by wind. The largest grains mobilized by wind will move via creep driven by impacts from abundant saltating finer grains. On Mars, 1- to 2-mm grains are driven by creep, leading to formation of megaripples observed at both Mars Exploration Rover landing sites [e.g., (24)]. The result of this process is a relatively thin surface layer of uniformly sized clasts due to size-dependent downwind (creep) migration rates, which differs in both geometry and the coarse grain size range (2 to 40 mm) within the martian conglomerates described here. The higher density of liquid fluids relative to air results in higher bed shear stress (and a buoyancy force on the particle), which can mobilize coarse sediment.

A number of factors influence the development of rounded clast perimeters in fluvial transport, including the original clast size, shape, and lithology, as well as the grain size of the bed material (21, 25). Sand commonly acts as an abrasive agent when transported with pebbles in fluvial systems, causing the coarser particles to round more rapidly (21, 22). The presence of coarse sand and rounded pebbles in the martian rocks is consistent with a highly abrasive flow. For clasts of the same size, lithology is the major factor affecting the rate of downstream rounding [e.g., (25–27)]. On the basis of published data for pebbles in natural streams and fluvial abrasion experiments for a range of compositions [e.g., (25–27)], and assuming an initial angular pebble, we estimate a minimum transport distance of a few kilometers to produce a rounded pebble surface. On Mars, the elastic collisions within the flow may have had lower energy due to the reduced gravity, resulting in lower abrasion rates and longer transport distances to achieve similarly rounded pebbles. Overall, the rounded pebbles of apparently diverse lithology within the martian conglomerates are strong evidence for sustained fluvial transport.

The grain size distribution can be used to estimate the critical shear stress for sediment mobility, and in turn the flow depth and mean velocity

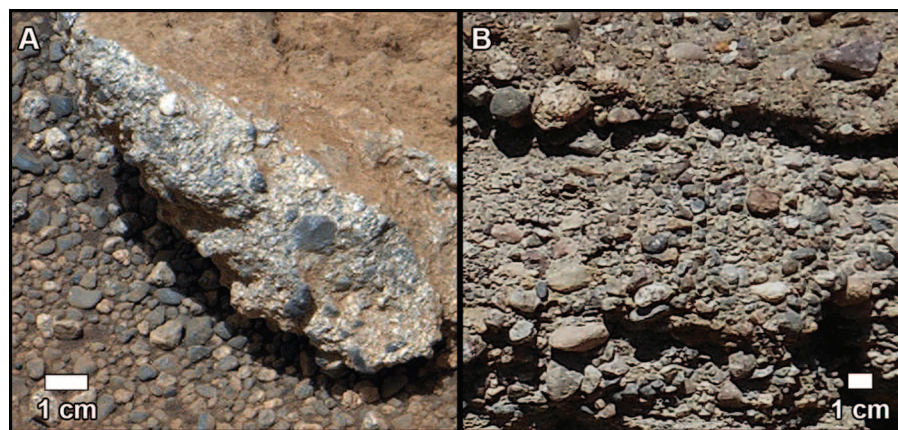


Fig. 2. Comparison of pebbles at Link and a terrestrial analog site. (A) Link was imaged with the 100-mm Mastcam on sol 27 (17). **(B)** Rounded clasts of similar size and shape are observed in comparably sized distal alluvial fan deposits on Earth, such as this example from the Atacama Desert, Chile.

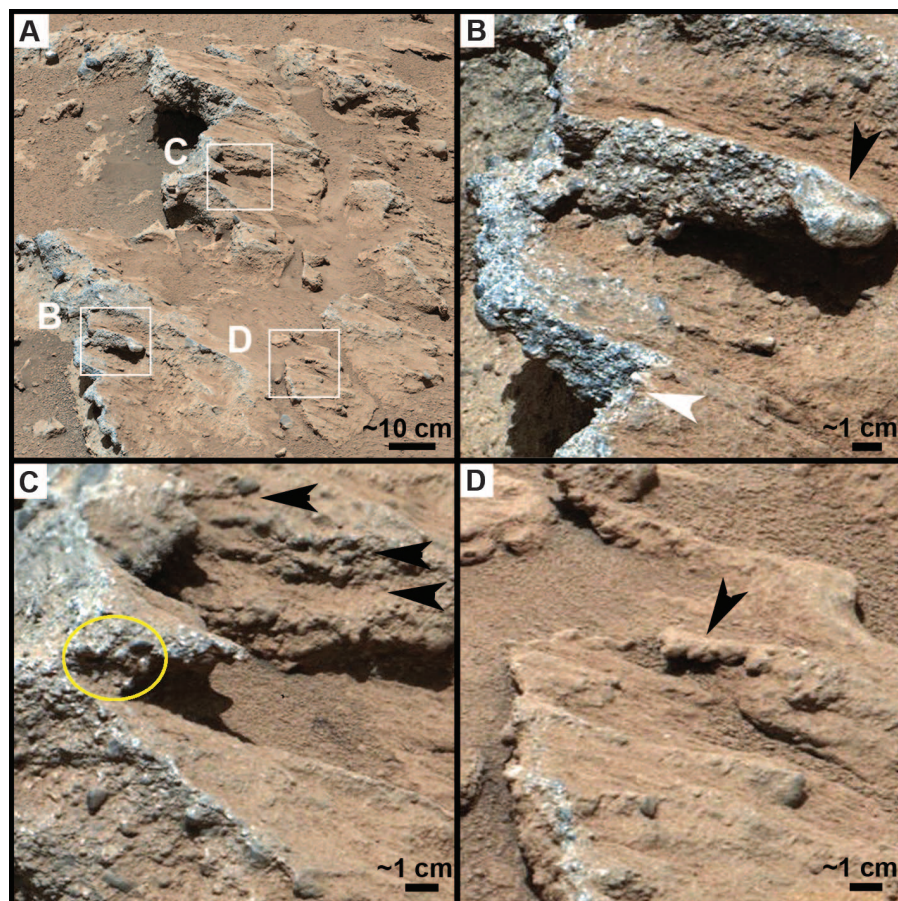


Fig. 3. Examples of sedimentary texture and fabric in the Hottah outcrop. (A) The Hottah outcrop has fractured and gently tilted ($\sim 30^\circ$) blocks, as seen in this mosaic of Mastcam images taken on sol 39 (17). **(B)** The perimeter of a well-rounded pebble protruding from the outcrop (upper black arrow, long axis ~ 3 cm) is smooth. White arrow points to parallel stratification. **(C)** In places, there are alternating protruding, pebble-rich layers (black arrows) and recessive layers. An example of a clast-supported pebble cluster is marked by the yellow circle. **(D)** Example of imbricated clasts.

assuming a water surface slope between 0.1 and 1% (17, 28–30) (tables S3 to S5). This range of slope values corresponds to the nearby alluvial fan slope (1%) and an approximate lower value (0.1%) for gravel-bedded streams [e.g., (31, 32)].

For the clast size distributions observed in the three conglomerates, the minimal flow depth (sufficient to initiate motion) is 0.03 to 0.9 m and the corresponding average flow velocity is estimated to be 0.20 to 0.75 m/s. In all cases, the estimated

Fig. 4. Cumulative grain size frequency plot. The x axis is the phi scale, which we have converted to millimeters (17). The grain size distributions for martian conglomerates and a terrestrial analog are normal in all cases, with most of the particles sizes clustered around the median value, consistent with fluvially transported sediment (41).

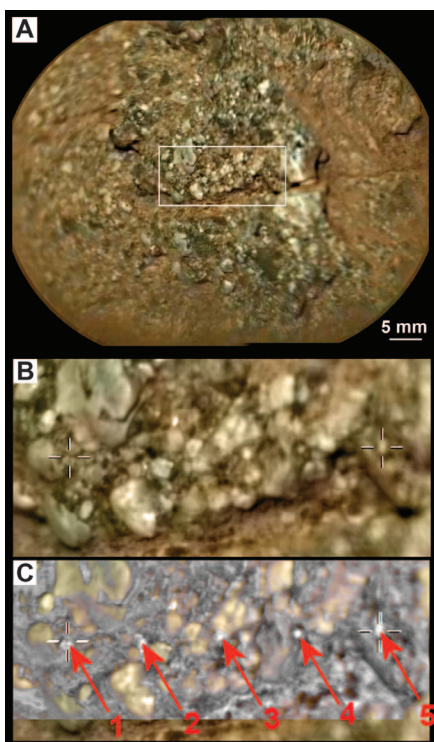
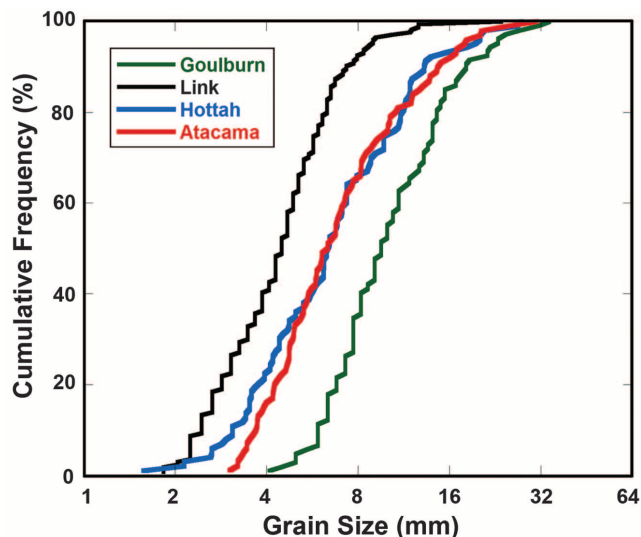


Fig. 5. Highest-resolution view of Link. (A) Mosaic of two RMI images (17) from a distance of 2.66 m to the Link outcrop, with color merged from Mastcam images. This composite image has a resolution of $\sim 50 \mu\text{m}$ per pixel. White box outlines the field of view in (B) and (C). (B) This enlarged view shows coarse sand grains in contact with light-toned pebbles, and rounded to sub-rounded grain shape. The interstitial component between resolvable grains appears dark-toned, suggests a mafic composition. The ends of a five-point LIBS line are marked by crosshairs. LIBS sampled mainly lighter grains with the exception of point 5, which sampled a darker area. In contrast to LIBS holes observed in some other rocks, LIBS shot points did not leave obvious marks on Link. (C) Difference map (from images acquired before and after laser activity) superimposed on the same view, showing the locations of the five ablated points.

threshold conditions correspond to subcritical flows where the gravitational force is greater than the inertial driving force [Froude number < 1 (17)]. Flows likely exceeded these threshold conditions.

Composition

The composition of the conglomerates is indicative of the sediment source and depositional environments. The Laser-Induced Breakdown Spectrometer (LIBS) of the ChemCam instrument (14–16) was used to determine elemental composition at the Link outcrop. Five points $\sim 400 \mu\text{m}$ in diameter spanning a distance of $\sim 15 \text{ mm}$ provided a compositional sampling of minerals in the coarse-grained rocks (Figs. 5 and 6). Laser shot points appear to have sampled predominantly the light-toned fraction of Link. The target is especially high in Si, K, and Na relative to typical martian basaltic rocks, and Rb is detected in concert with K at the 100- to 200-ppm level (17). The partial least squares (PLS) processed results show a composition corresponding to high silica and high alkaline content (table S6). The high Si content and normative plagioclase and orthoclase suggest a substantial feldspar component, consistent with the presence of light-toned grains [see (33) for additional detail]. The presence of alkaline elements (i.e., mobile cations such as Ca, Na, and K) in Link indicates that prolonged aqueous alteration has not occurred (table S6).

A Fe-, Ti-, and Cr-rich component identified in point 5 (Fig. 6B) is similar in composition to typical martian regolith [approximately basalt composition (17)]. However, the RMI images of Link (Fig. 5) confirm that the rock is largely free of a loose surface coating. In addition, a thicker dust mantling here is discarded as a possibility because of the compositional difference between point 5 and average dust (table S6). The phase with high Fe and Ti abundance may correspond to fine basaltic grains that were transported with larger clasts, reflecting different provenance, or to an iron-rich cement.

In addition, all Link spectra display a hydrogen peak visible at 656 nm, consistent with the presence of a low proportion of hydrated mineral(s). This peak is present in all points but seems to be higher for the first 25 shots at point 5 (Fig. 6B), corresponding to the Fe-, Ti-, and Cr-bearing component. The depletion of mobile elements (e.g., Na) relative to aluminum in this phase may be consistent with limited alteration. We cannot determine whether the observed hydration is related to in situ aqueous alteration of fine grains, or to minor alteration phases that were already present in the martian crust and transported as fines with the larger clasts. The isolated rock exposures and consistent thickness of beds suggests localized induration after flows ceased.

Overall, the chemical data are consistent with a rock comprising first-cycle clastic sediments with preservation of coarse feldspar grains and minimal alteration products. We conclude that clast size and shape developed predominantly from mechanical rock breakdown by fluvial abrasion, in contrast to terrestrial rivers where the development of weathering rinds is a secondary mechanism contributing to clast diminution and form [e.g., (34)].

Stratigraphic Interpretation

The conglomerates have a complex geologic setting: The ancient impact basin they lie within formed approximately 3.6 to 3.8 billion years ago, around the Noachian-Hesperian transition (35, 36), and may have filled completely with sediment before being eroded to the current morphology through aeolian erosion (36). The Bradbury conglomerates are within the crater-fill stratigraphy and document the role of fluvial processes in sedimentation within Gale crater.

Multiple fluvial pathways have been identified at Gale crater from orbital images [e.g., (10)], but none can be connected with confidence to the conglomerates. Both Aeolis Mons and the crater rim show geomorphic evidence for fluvial incision (10, 37) (Fig. 1) and could have been sediment sources for the conglomerates. For example, the conglomerates are located downslope of a large, crater rim-sourced alluvial fan ($\sim 80 \text{ km}^2$). The transport distances across the alluvial fan ($\sim 14 \text{ km}$) and from its drainage basin ($> 40 \text{ km}$) are consistent with the rounded clast observations. The distal Peace Vallis alluvial fan slope ($\sim 1\%$ gradient) can be projected across a topographic depression $\sim 5 \text{ km}$ to the conglomerate outcrops. However, there is no evidence to date, except topography, indicating that the Peace Vallis fan extended to this area. In the absence of contact relationships between the Bradbury Rise conglomerates and mapped geomorphic features interpreted as water-formed, the overall stratigraphic context and relative age of the conglomerates are uncertain. Thus, the most parsimonious interpretation is that the conglomerates are distal alluvial fan deposits of unknown age.

Despite the uncertainty in their stratigraphic context, the Bradbury conglomerates constitute a record of past conditions at Gale crater that contrast

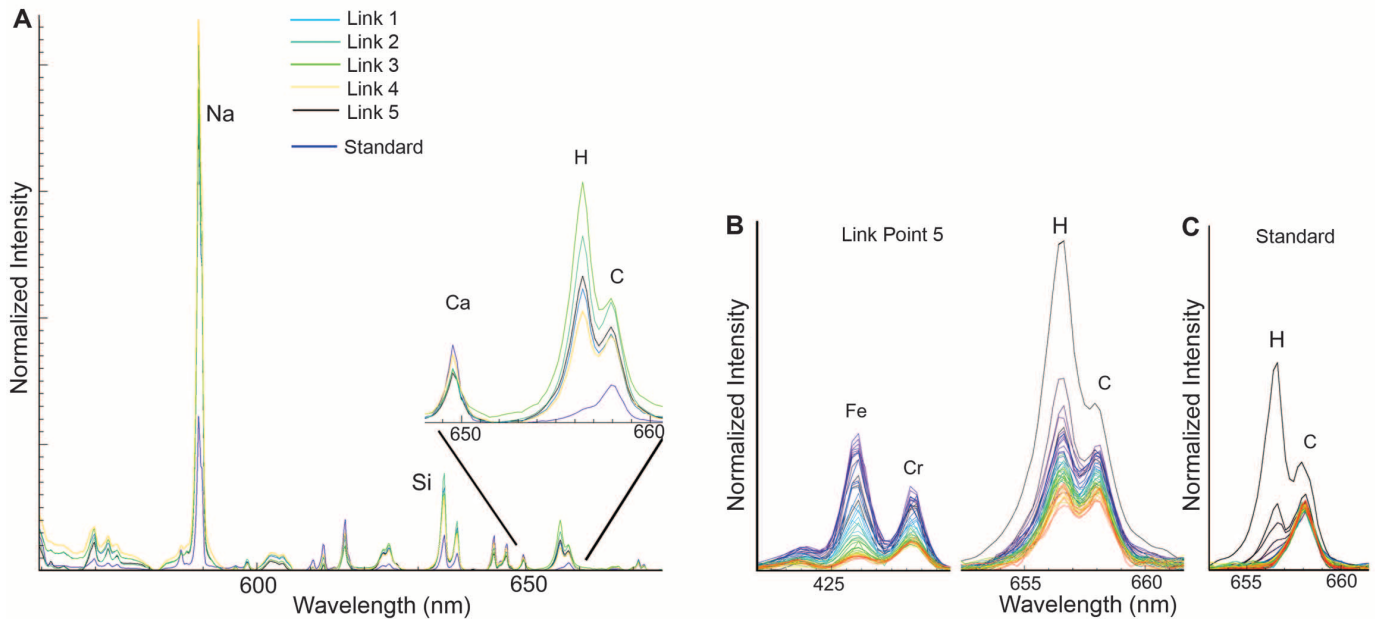


Fig. 6. Emission spectra from Link. (A) ChemCam averaged spectra (17) in selected wavelengths for five points (Fig. 5C) on the Link outcrop and an anhydrous rover-mounted calibration standard [norite composition (42) in navy blue]. All Link spectra have higher Si and Na than the norite standard (in contrast, Ca is slightly higher in the norite), in agreement with quantitative analyses (table S6). Enlargement of the hydrogen line region at 656 nm shows detection of hydrogen in the average spectra of all points at Link. The emission

line at 658 nm corresponds to atmospheric carbon and varies only because of the correlated variations in hydrogen. (B) Shot-by-shot data over the 50 shots at point 5 (black, shot 0; red, shot 50). The first half of these shots have higher Fe, Cr, and H emission lines than the second half, corresponding to a progressive change in composition with depth (table S6). (C) By comparison, the onboard norite standard shows H only in the first five shots (surfacial dust contribution), whereas most of the target is dry, as expected.

with the modern martian environment, where liquid water is unstable under current atmospheric conditions (38). These ancient fluvial deposits indicate sustained liquid water flows across the landscape—a finding that raises prospects for the former presence of habitable environments on Mars.

References and Notes

1. M. C. Malin, K. S. Edgett, *Science* **302**, 1931 (2003).
2. J. M. Moore, A. D. Howard, *J. Geophys. Res.* **110**, E04005 (2005).
3. Mars Channel Working Group, *Geol. Soc. Am. Bull.* **94**, 1035 (1983).
4. P. H. Smith *et al.*, *Science* **278**, 1758 (1997).
5. Rover Team, *Science* **278**, 1765 (1997).
6. Rocks at the Pathfinder site with possible sockets and knobs were proposed as candidate conglomerates, but low image quality made this interpretation equivocal.
7. S. W. Squyres *et al.*, *Science* **306**, 1709 (2004).
8. J. P. Grotzinger *et al.*, *Earth Planet. Sci. Lett.* **240**, 11 (2005).
9. J. P. Grotzinger *et al.*, *Geology* **34**, 1085 (2006).
10. R. B. Anderson, J. F. Bell, *Mars* **5**, 76 (2010).
11. J. P. Grotzinger *et al.*, *Space Sci. Rev.* **170**, 5 (2012).
12. A sol is a martian day.
13. Names have been assigned to areographic features and rocks by the MSL team for planning and operations purposes. These names are not formally recognized by the International Astronomical Union.
14. Cameras on Curiosity's remote sensing mast include four monochrome navigation cameras, each with a 45° field of view (FOV), and two color cameras (Bayer pattern color filter array) that constitute the stereo Mastcam instrument. The left camera has a 34-mm focal length with 15° FOV; the right camera has a 100-mm focal length and 5° FOV. At a distance of 2 m, the Mastcam pixel scales are 440 and 148 μm , respectively. The ChemCam instrument is a package of a Laser-Induced Breakdown Spectrometer (LIBS) coupled to a Remote Micro-Imager (RMI). The full FOV for each RMI is 20 milliradians. The Mars Hand Lens Imager (MAHLI) and Alpha-Proton X-ray Spectrometer (APXS) instruments were not commissioned for tactical operations when the conglomerates were encountered.
15. R. C. Wiens *et al.*, *Space Sci. Rev.* **170**, 167 (2012).
16. S. Maurice *et al.*, *Space Sci. Rev.* **170**, 95 (2012).
17. See supplementary materials on Science Online.
18. R. A. Yingst, A. F. C. Haldemann, K. L. Biedermann, A. M. Monhead, *J. Geophys. Res.* **112**, E06002 (2007).
19. J. B. Garvin, P. J. Mouginis-Mark, J. W. Head, *Moon Planets* **24**, 355 (1981).
20. R. A. Yingst *et al.*, *J. Geophys. Res.* **113**, E12S41 (2008).
21. R. L. Folk, *The Petrology of Sedimentary Rocks* (Hemphills, Austin, TX, 1980).
22. W. C. Krumbein, L. L. Sloss, *Stratigraphy and Sedimentation* (Freeman, New York, 1963).
23. P. J. Whiting, W. E. Dietrich, L. B. Leopold, T. G. Drake, R. L. Shreve, *Geology* **16**, 105 (1988).
24. D. J. Jerolmack, D. Mohrig, J. P. Grotzinger, D. A. Fike, W. A. Watters, *J. Geophys. Res.* **111**, E12S02 (2006).
25. H. H. Mills, *J. Sediment. Petrol.* **49**, 295 (1979).
26. N. S. Davies, R. K. Vessell, R. C. Miles, M. G. Foley, S. B. Bonis, in *Fluvial Sedimentology*, A. D. Miall, Ed. (Canadian Society of Petroleum Geologists, Calgary, 1977), Memoir 5, pp. 61–84.
27. J. Lewin, P. A. Brewer, *Earth Planet. Sci. Lett.* **27**, 145 (2002).
28. Scaling analysis suggests that Mars' lower gravity has only a minor effect on fluvial gradients at the threshold of motion and bedform configuration. Therefore, it is appropriate to compare terrestrial fluvial bedforms and gradients to their martian counterparts.
29. V. T. Chow, *Open-Channel Hydraulics* (Blackburn, Caldwell, NJ, 1959).
30. P. D. Komar, *Icarus* **42**, 317 (1980).
31. G. Parker, P. R. Wilcock, C. Paola, W. E. Dietrich, J. Pitlick, *J. Geophys. Res.* **112**, F04005 (2007).
32. R. S. Anderson, S. P. Anderson, *Geomorphology: The Mechanics and Chemistry of Landscapes* (Cambridge University Press, Cambridge, 2010).
33. R. C. Wiens *et al.*, *44th Lunar and Planetary Science Conference*, Abstract 1363 (2013); www.lpi.usra.edu/meetings/lpsc2013/pdf/1363.pdf.
34. P. L. Heller *et al.*, *Geology* **29**, 971 (2001).
35. The Noachian is a geologic system on Mars representing the oldest period of the planet's geologic history, characterized by high impact rates.
36. B. J. Thomson *et al.*, *Icarus* **214**, 413 (2011).
37. M. C. Malin, K. S. Edgett, *Science* **290**, 1927 (2000).
38. R. M. Haberle *et al.*, *J. Geophys. Res.* **106**, 23317 (2001).
39. D. E. Smith *et al.*, *J. Geophys. Res.* **106**, 23689 (2001).
40. A. S. McEwen *et al.*, *J. Geophys. Res.* **112**, E05S02 (2007).
41. K. Bunte, S. R. Abt, *U.S. Department of Agriculture General Technical Report RMRS-GTR-74* (2001).
42. S. M. Fabre *et al.*, *Spectrochim. Acta B* **66**, 280 (2011).

Acknowledgments: We thank K. Tanaka and L. Kestay (USGS-Flagstaff) and four anonymous referees for constructive reviews of this manuscript. This research was carried out for the Jet Propulsion Laboratory, California Institute of Technology, under a contract with NASA under the Mars Program Office, including JPL contracts 1449884 (R.M.E.W.) and 1273887 (Malin Space Science Systems). Work in France was carried out with funding from the Centre National d'Etudes Spatiales. Work in the UK was funded by the UK Space Agency. Work in Denmark was funded by the Danish Council for Independent Research/Natural Sciences (FNU grants 12-127126 and 11-107019) and the TICRA Foundation. Work in Germany was partly funded by Deutsche Forschungsgemeinschaft grant GO 2288/1-1. Data in this manuscript are available from the NASA Planetary Data System. This is PSI contribution 603.

Supplementary Materials

www.sciencemag.org/cgi/content/full/340/6136/1068/DC1
Methods
Supplementary Text
Figs. S1 to S3
Tables S1 to S6
References (43–56)

4 March 2013; accepted 7 May 2013
10.1126/science.123717

Martian Fluvial Conglomerates at Gale Crater

R. M. E. Williams, J. P. Grotzinger, W. E. Dietrich, S. Gupta, D. Y. Sumner, R. C. Wiens, N. Mangold, M. C. Malin, K. S. Edgett, S. Maurice, O. Forni, O. Gasnault, A. Ollila, H. E. Newsom, G. Dromart, M. C. Palucis, R. A. Yingst, R. B. Anderson, K. E. Herkenhoff, S. Le Mouélic, W. Goetz, M. B. Madsen, A. Koefoed, J. K. Jensen, J. C. Bridges, S. P. Schwenzer, K. W. Lewis, K. M. Stack, D. Rubin, L. C. Kah, J. F. Bell III, J. D. Farmer, R. Sullivan, T. Van Beek, D. L. Blaney, O. Pariser, R. G. Deen and MSLS Science Team

Science **340** (6136), 1068-1072.
DOI: 10.1126/science.1237317

Going to Mars

The Mars Science Laboratory spacecraft containing the Curiosity rover, was launched from Earth in November 2011 and arrived at Gale crater on Mars in August 2012. **Zeitlin *et al.*** (p. 1080) report measurements of the energetic particle radiation environment inside the spacecraft during its cruise to Mars, confirming the hazard likely to be posed by this radiation to astronauts on a future potential trip to Mars. **Williams *et al.*** (p. 1068, see the Perspective by **Jerolmack**) report the detection of sedimentary conglomerates (pebbles mixed with sand and turned to rock) at Gale crater. The rounding of the rocks suggests abrasion of the pebbles as they were transported by flowing water several kilometers or more from their source.

ARTICLE TOOLS

<http://science.sciencemag.org/content/340/6136/1068>

SUPPLEMENTARY MATERIALS

<http://science.sciencemag.org/content/suppl/2013/05/30/340.6136.1068.DC1>

RELATED CONTENT

<http://science.sciencemag.org/content/sci/340/6136/1055.full>
<file://contentpending:yes>

REFERENCES

This article cites 39 articles, 11 of which you can access for free
<http://science.sciencemag.org/content/340/6136/1068#BIBL>

PERMISSIONS

<http://www.sciencemag.org/help/reprints-and-permissions>

Use of this article is subject to the [Terms of Service](#)